JOURNAL OF THERMOPHYSICS AND HEAT TRANSFER
Vol. 17, No. 2, April–June 2003

Thermophysics Characterization of Multiply Ionized Air Plasma Absorption of Laser Radiation

Ten-See Wang*
NASA Marshall Space Flight Center, Huntsville, Alabama 35812
and
Robert Rhodes†
University of Tennessee Space Institute, Tennessee 37388

Thermodynamic properties of multiply ionized air plasma atoms are computed using hydrogenic approximation of the electronic partition function for temperatures up to 1,500,000 K, to study the impact of multiple ionization of air plasma on the inverse Bremsstrahlung absorption of laser radiation. Three formulas of inverse Bremsstrahlung absorption are investigated, and a general electron–ion inverse Bremsstrahlung formula is derived for multispecies, multiple ionization absorption. The computed double ionization absorption coefficients agree reasonably well with those of literature for 1, 10, and 100 atm. The importance of multiple ionization modeling is demonstrated by finding that the area under the full ionization absorption curve is twice that of single ionization. The effect of pressure on fully ionized air plasma absorption is computed for five pressures: 0.01, 0.1, 1, 10, and 100 atm.

Nomenclature

a_0	=	first Bohr radius
a_1–a_7	=	coefficients for thermodynamic functions
b_1, b_2	=	thermodynamic function integration constants
C_p	=	molar heat capacity at constant pressure
c	=	light velocity in vacuum
D_s	=	Debye shielding distance
E	=	ionization potential
g	=	Gaunt factor
H	=	molar enthalpy at temperature for standard state
H_0	=	molar enthalpy at 0 K for standard state
h	=	Plank constant
$\hbar$	=	Plank constant/2π
I	=	laser intensity
M	=	molecular or atomic weight
m_e	=	electron mass
n	=	nth state of excitation energy
n_a, n_m	=	number density of atoms and molecules
n_e, n_i	=	number density of electron and ions
p	=	pressure
Q	=	partition function
q	=	proton charge
R	=	universal gas constant
S	=	entropy at temperature for standard state
s_c	=	Sackur–Tetrode constant
s_i	=	optical path length of the ith ray
T	=	electron temperature
Z	=	ion charge
α	=	fine structure constant
ΔE	=	lowering of the ionization potential
ε_0	=	permittivity of free space
κ	=	absorption coefficient
κ_B	=	Boltzmann's constant
μ	=	real refractive index
ω	=	angular frequency

Subscripts

e	=	electron
f	=	formation
H	=	hydrogen atom
i	=	ith state
s	=	species

Presented as Paper 2002-2203 at the AIAA 33rd Plasmadynamics and Lasers Conference, Maui, HI, 20–23 May 2002; received 1 July 2002; revision received 30 September 2002; accepted for publication 1 October 2002.

*Staff, Applied Fluid Dynamics Analysis Group, Space Transportation Directorate. Senior Member AIAA.

†Research Scientist, Center for Laser Applications. Senior Member AIAA.

Introduction

IN the 1970s, Kantrowitz[1] first suggested a new possibility for dramatic cost reductions in mass launching to Earth orbit with a ground-based high-power laser. Since then, a propulsion system supported by a laser-sustained plasma has been the subject of much research.[2–5] The main advantage gained by laser propulsion over chemical propulsion is the low-weight system obtained from decoupling the energy source from the vehicle and the high specific impulse resulting in low fuel consumption. In addition, the propellant temperature reachable during laser propulsion can be several orders of magnitude higher than the flame temperature of a combustion process.

Several airbreathing laser propulsion concepts have been demonstrated in the past few years. For example, recent publications show that a spin-stabilized Myrabo lightcraft reached 71 m in record height during vertical free flights outdoors,[6] whereas a different parabolic flyer (design) was propelled from the ground of the laboratory to its 8-m-high ceiling.[7] High-energy CO_2 lasers were used in both tests.

Researchers using computational plasma aerodynamics have also been making progress in the field of laser propulsion. For example, Molvik et al.[8] considered the interaction between a continuous laser beam and a flowing hydrogen gas using a structured-grid formulation and constant absorptivity. Jeng and Keefer[9] conducted a similar analysis with an expression for the absorption coefficient at a CO_2 laser wavelength of 10.6 μm, which considered both electron–ion and electron–neutral inverse Bremsstrahlung. Conrad et al.[10] modeled a continuous optical discharge stabilized by nitrogen gas flows in a weakly focused laser beam, by use of an absorption coefficient formula at 10.6 μm ignoring the second ionization of atoms.[10] Recently, Wang et al. performed transient performance computations[11] on a Myrabo lightcraft (energized by a pulsed laser beam) using

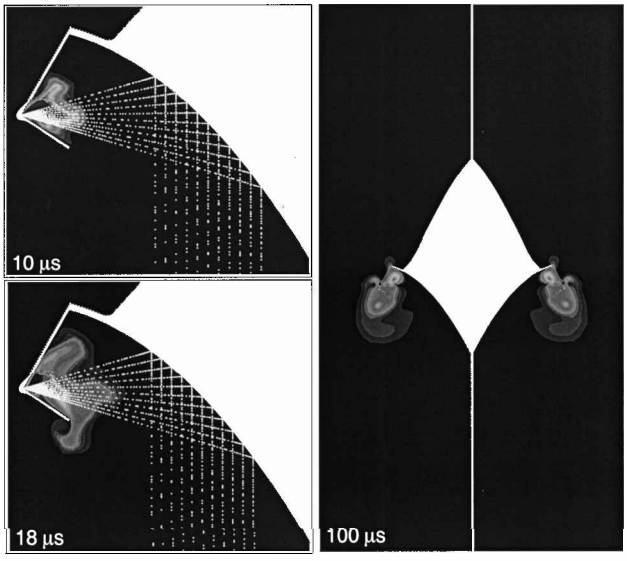

Fig. 1 Computational plasma aerodynamics computed electron temperature contours and laser ray traces for a Myrabo lightcraft; contours scale: 10 μs, 7600–109,640, maximum 195,575; 18 μs, 8900–129,300, maximum 137,910; and 100 μs, 890–9190, maximum 9780.

an unstructured-grid formulation and the same single ionization absorption formula used by Conrad et al.[10]

In a computational plasma aerodynamics study, using the modeling of a Myrabo lightcraft[11] as an example, the focusing of the laser radiation is solved first, followed by computing the initial air breakdown and the creation of seed free electrons. When enough seed electrons are produced, they absorb more photons, which results in more air breakdown and produces more free electrons. An avalanche of free electrons soon follows, and a strong shock wave is generated. These are all solved with transport equations of continuity, energy, momentum, and species continuity, along with physical models such as finite-rate chemistry, high-temperature thermodynamics, beam attenuation through absorption, beam refraction, and nonequilibrium radiation. The computational model then computes the subsequent traveling of the shock wave through air, the heating and ionizing (such that the air plasma becomes capable of absorbing more laser radiation), and most important the thrust of the lightcraft. Figure 1 shows snapshots of the computed electron temperature contours and laser beam traces at elapsed times of 10, 18, and 100 μs (Ref. 11). It can be seen that the laser beam reflects specularly on the optical surface and focuses onto a focal ring on the shroud, where the breakdown of air occurs. The temperature contours in Fig. 1 also show the growth of the plasma front. The "protrusion" of the plasma front at 10 and 18 μs indicates that the plasma front (and the shock wave) is propagating up the beam, a result of successive heating and ionizing of the medium (air) such that the plasma front becomes capable of absorbing more laser energy and propagates further. At 100 μs when the laser is off, the optical breakdown is not being maintained by the laser irradiation, and the electron temperature decreases, as well as other plasma properties such as ions, neutrals, and electron number densities. The shock wave moves out of the shroud region rapidly, leaving the plasma cloud behind and trailing in a slow, vortical motion. Figure 1 is an indication of the potential ability of the computational plasma aerodynamics in describing the optical breakdown phenomenon and energy conversion processes associated with laser propulsion. It also indicates the importance of a realistic absorption model because the propulsion physics start with the absorption of laser energy. It goes without saying that the accuracy of the absorption model affects that of the computed performance and efficiency.

Other than the constant absorption coefficient used by Molvik et al.,[8] all of the variable absorption formulas used by the aforementioned modeling efforts[9–11] are of single ionization. Although applying single ionization formula to a hydrogen plasma[9] is reasonable, there is room for improvement when it is applied to nitrogen and air plasmas[10,11] because the atomic numbers of nitrogen and oxygen atoms are eight and nine, respectively. Given that a simplified procedure for computing the effect of multiple ionization was already reported by Zel'dovich and Raizer[12] in the 1960s and a single ionization formula formulated by Raizer and Tybulewicz[13] in the 1970s was still being used in the 1990s,[10] it is speculated that the difficulty resides in the scarcity of reliable high-temperature thermodynamic properties for the multiply ionized air atoms. For example, the standard thermodynamics library of Gordon and McBride[14] carries only singly ionized atoms with maximum applicable temperature up to 20,000 K, whereas the maximum temperature during optical breakdown was computed to 200,000 K (Ref. 11). To understand the impact of multiply ionized atoms on the absorption of laser radiation, reliable high-temperature thermodynamic properties for the multiply ionized air atoms have to be developed, and that is the motivation of this study.

Thermophysics Characterization of Multiply Ionized Air Plasma

Hydrogenic Approximation of the Partition Function

The high-temperature thermodynamic properties of the multiply ionized atoms can be expressed in terms of partition functions, following those formulated for monatomic gases.[14] For example,

$$\frac{C_p}{R} = T^2\frac{\mathrm{d}^2 \ell_n Q}{\mathrm{d}T^2} + 2T\frac{\mathrm{d}(\ell_n Q)}{\mathrm{d}T} + \frac{5}{2} \tag{1}$$

$$\frac{H - H_0}{RT} = T\frac{\mathrm{d}(\ell_n Q)}{\mathrm{d}T} + \frac{5}{2} \tag{2}$$

$$\frac{S}{R} = T\frac{\mathrm{d}(\ell_n Q)}{\mathrm{d}T} + \ell_n Q + \frac{3}{2}\ell_n M + \frac{5}{2}\ell_n T + s_c \tag{3}$$

In this study, the energy levels of ionized atoms is characterized with the method of hydrogenic approximation.[12,15] That is, the multiply ionized atoms are treated as hydrogenlike atoms, represented by a system consisting of a positive nucleus with a charge Z and a single electron. The hydrogenlike electronic partition function takes the form

$$Q_i = \sum_n 2n^2 \exp\left[-\frac{E_i}{\kappa_B T}\left(1 - \frac{1}{n^2}\right)\right] \tag{4}$$

where the summation is truncated when $[E_i(1 - 1/n^2)]$ is greater than $[E_i - \Delta E]$. The lowering of the ionization potential is written as[15]

$$\Delta E_{z-1} = Z\left(q^2 / D_s\right) \tag{5}$$

where

$$D_s = \frac{1}{q}\sqrt{\kappa_B T \Big/ \left[n_e + \sum_{s,z}(Z-1)^2 n_{s,z-1}\right]} \tag{6}$$

Thermochemical Equilibrium Systems

For convenience, two thermochemical equilibrium systems are employed in this study. The first system couples the aforementioned hydrogenic approximation method with an equilibrium computational procedure solving the Saha equations (see Ref. 15). The Saha equilibrium relationship combined with the constancy of the elemental ratios and the overall conservation of mass provide equations that are linear in species composition if the electron composition is assumed. Electrical neutrality provides an equation that is used to adjust the electron composition iteratively. This simple procedure works with atoms and ions, but the equations are nonlinear if molecular dissociation is included. Therefore, the first system is used to generate the thermodynamic properties for the multiply ionized atoms for use in the more general second system. It is also used to provide equilibrium species composition for studying the effect of pressure on absorption of laser radiation.

This computational procedure originally uses the assigned internal energy and density as input. The internal energy of a given

species is a function of the temperature, partition function, energy of ionization, and reference point energy. This reference is arbitrary, but it is chosen to be the energy of formation of the element from its reference state as defined by Gordon and McBride.[14] The result of the computation is a table of thermodynamic properties for multiply ionized atoms as a function of temperatures and densities. The contribution of the authors to this development included adding an assigned temperature and pressure option for this work, using a correct form for computing the lowering of the ionization energy and modifying the matrix inversion routine such that thermodynamic properties can be computed at low temperatures without resorting to a cutoff temperature procedure. When full ionization is considered, 16 species, e^-, N, N^+, N^{+2}, N^{+3}, N^{+4}, N^{+5}, N^{+6}, O, O^+, O^{+2}, O^{+3}, O^{+4}, O^{+5}, O^{+6}, and O^{+7}, are considered in the first system.

The thermodynamic properties of the multiply ionized N and O atoms generated in the first system are curve fitted into polynomials and coupled into the second system, where thermodynamic polynomials for the molecules and other ions are collected or generated from other sources. Therefore, the second system is general and designed for computational plasma aerodynamics analysis using either finite-rate or equilibrium chemistry. In this study, a general minimization of the free energy procedure, similar to that described by Gordon and McBride,[16] is employed to provide equilibrium properties from the second system. Note that a table lookup method is equally useful for computational purposes.

In Ref. 11, the initial free electrons for plasma ignition and the subsequent avalanche of free electrons necessary for the optical breakdown were generated through the nonequilibrium finite-rate air breakdown chemistry submodel, where Park's multitemperature air chemistry mechanism[17] was used. This mechanism is composed of the dissociation, NO exchange, associative ionization, charge exchange, electron impact ionization, and radiative recombination reactions. The 11 air plasma species used in this mechanism define the (second) thermochemical system for single ionization environment: N_2, O_2, NO, NO^+, N, N^+, O, O^+, N_2^+, O_2^+, and e^-. N_2, O_2, and NO are neutral molecules; N and O are neutral atoms; and NO^+, N^+, O^+, N_2^+, and O_2^+ are single ions. To consider multiply ionized air plasma atoms, up to quadruple ionization, for example, six additional ions, N^{+2}, O^{+2}, N^{+3}, O^{+3}, N^{+4}, and O^{+4}, must be added, and their thermodynamic properties must be characterized.

Thermodynamic Function Generation

For general computational plasma aerodynamics analysis, the three thermodynamic functions (polynomials) of heat capacity, enthalpy, and entropy as functions of temperature must be generated. The standard form of Gordon and McBride[14] is used:

$$C_p/T = a_1T^{-2} + a_2T^{-1} + a_3 + a_4T + a_5T^2 + a_6T^3 + a_7T^4 \quad (7)$$

$$H/RT = -a_1T^{-2} + a_2T^{-1}\ln T + a_3 + a_4(T/2) + a_5(T^2/3) + a_6(T^3/4) + a_7(T^4/5) + b_1/T \quad (8)$$

$$S/R = -a_1(T^{-2}/2) - a_2T^{-1} + a_3\ln T + a_4T + a_5(T^2/2) + a_6(T^3/3) + a_7(T^4/4) + b_2 \quad (9)$$

These coefficients are obtained through a least-square curve-fit procedure for each temperature interval of a three-temperature interval format, following Gordon and McBride.[14] Unlike Gordon and McBride, where the three temperature intervals are identical for all of the species and maximum temperature is 20,000 K, the three temperature intervals are made different for different species to achieve the best fit of the generated thermodynamic properties over a much wider range of temperatures (up to 1,500,000 K). To construct the enthalpy curve, the heat of formation of multiply ionized ions at a reference state needs to be estimated. This is accomplished by writing an ionization reaction, for example, for N^+,

$$N \rightarrow N^+ + e^- \quad (10)$$

Table 1 Comparison of thermodynamic data of multiply ionized air species

	$H_{f,298\ K}$, kcal/mol		$S_{f,298\ K}$, cal/(mol · K)	
Species	This work	Ref. 18	This work	Ref. 18
N	112.9732[a]	112.9732	35.2349	36.6396
N^+	448.0539	449.8382	35.2349	38.1924
N^{+2}	1,130.5068	——	35.2349	——
N^{+3}	2,224.2118	——	35.2349	——
N^{+4}	4,010.3091	——	35.2349	——
N^{+5}	6,265.7038	——	35.2349	——
N^{+6}	18,993.8093	——	35.2349	——
N^{+7}	34,371.7729	——	35.2349	——
O	59.5554[a]	59.5554	35.6292	38.4938
O^+	373.5119	374.9503	35.6292	37.0361
O^{+2}	1,183.1479	——	35.6292	——
O^{+3}	2,448.8901	——	35.6292	——
O^{+4}	4,233.6960	——	35.6292	——
O^{+5}	6,859.7549	——	35.6292	——
O^{+6}	10,044.0586	——	35.6292	——
O^{+7}	27,088.9849	——	35.6292	——
O^{+8}	47,175.3732	——	35.6292	——

[a]Reference 18.

The heat of reaction of this ionization reaction is the ionization potential. The heat of formation of N^+ takes the form

$$H_{f,N^+} = H_{f,N} + E - H_{f,e^-} \quad (11)$$

The heat of formations of N and O from Gurvich et al.[18] are used as the basis for computing those for the multiply ionized atoms, as shown in Table 1. It can be seen that the computed heat of formations for singly ionized N^+ and O^+ are comparable to those published by Gurvich et al. In addition, the computed entropy of formations using hydrogenic approximation of the partition function for N, O, N^+, and O^+ are also comparable to those published by Gurvich et al.

The thermodynamic functions of the rest of the air plasma species, N_2, O_2, NO, NO^+, N_2^+, O_2^+, and e^-, are obtained from Gordon and McBride,[16] where the computed data (up to 20,000 K) from Gurvich et al.[18] were curve fitted. The thermodynamic functions for molecular species N_2, O_2, and NO are regenerated up to 50,000 K by incorporating the specific heat data computed by Jaffe.[19]

Laser Absorption

In computational plasma aerodynamics modeling[11] of the laser lightcraft flowfield where geometric optics is used to simulate the local intensity of the laser beam, the laser beam can be split into a number of individual rays. In the presence of absorption, the local intensity of each ray follows Beer's law:

$$\frac{dI_i}{ds_i} = -\kappa I_i \quad (12)$$

Through inverse Bremsstrahlung absorption, the rays are attenuated by free electrons in their path. The three types of inverse Bremsstrahlung absorption, depending on what kind of particle the electron is near when a photon is absorbed, are electron–ion (free–free), electron–atom, and electron–molecular absorptions. According to Raizer and Tybulewicz,[13] the long-wavelengthinfrared radiation of a CO_2 laser at 10.6 μm is absorbed mainly by free electrons when it collide with ions. Hughes[20] gives a theoretical derivation of the electron–ion inverse Bremsstrahlung absorption coefficient for radiation at frequency ω,

$$\kappa_\omega = \frac{n_e n_i Z^2 q^6 g[1 - \exp(-\hbar\omega/\kappa_B T)]}{\mu 6\varepsilon_0^3 c\hbar\omega^3 m_e^2}\left(\frac{m_e}{6\pi\kappa_B T}\right)^{\frac{1}{2}} \quad (13)$$

The advantage of Hughes[20] formula is its flexibility, that is, it can be used for radiation in any wavelength. In contrast, Raizer and Tybulewicz[13] started with a different formulation from that of Hughes,[20] corrected for stimulated emission in the single ionization

range, assumed $\hbar\omega/\kappa_B T \ll 1$, omitted the factor affecting only the photoionization, and substituted $\hbar\omega$ for CO_2 laser wavelength, to arrive a formula of electron–ion inverse Bremsstrahlung absorption coefficient

$$\kappa_{CO_2} = \frac{10.4 p_e^2 g}{(T/10^4)^{\frac{7}{2}}} \tag{14}$$

where

$$g = 0.55\,\ell n\left[27(T/10^4)^{\frac{4}{3}} p_e^{-\frac{1}{3}}\right] \tag{15}$$

Note the formula (14) does not take the second ionization (or higher) into account. Also, electron pressure is used in lieu of electron number density. Both described formulas (13) and (14) consider the electron–ion inverse Bremsstrahlung absorption only. On the other hand, Mertogul[21] computed the absorption coefficient for hydrogen plasmas using all three types of inverse Bremsstrahlung. The formula used for the computation of electron–ion inverse Bremsstrahlung absorption coefficient is that given by Stallcop,[22]

$$\kappa_\omega = n_e n_i (256/3)(\pi/3)^{\frac{1}{2}} \pi^2 \alpha a_0^5 (E_H/\hbar\omega)^3 (E_H/\kappa_B T) \times \{1 - \exp[-(\hbar\omega/\kappa_B T)]\} g \tag{16}$$

in which the free–free Gaunt factor was curve fitted from reported data of Karzas and Latter[23] at a wavelength of 10.6 μm.

The expression used for the electron–atom inverse Bremsstrahlung absorption coefficient in the infrared limit is that given by Stallcop,[24]

$$\kappa_\omega = n_e n_a \kappa_B T (2.15 \times 10^{-29})(E_H/\hbar\omega)^2 \left[\exp\left(-4.862 k_T \times \left(1 - 0.2096 k_T + 0.017 k_T^2 - 0.00968 k_T^3\right)\right)\Big/ k_T\right] \tag{17}$$

and

$$\kappa_T = (\kappa_B T/E_H)^{\frac{1}{2}} \tag{18}$$

The expression used for the electron–molecule inverse Bremsstrahlung absorption coefficient is that given by Caledonia et al.[25] from the work of Dalgarno and Lane,[26]

$$\kappa_\omega = n_e n_m (4.51 \times 10^{-44})\left(D\Big/T^{\frac{3}{2}}\{1 - \exp[-(\hbar\omega/\kappa_B T)]\}\right) \tag{19}$$

where D is a complicated power series represented as a function of $\hbar\omega/\kappa_B T$ and was given by Mertogul in the Appendix of Ref. 21. For a CO_2 laser wavelength of 10.6 μm, this expression of electron–molecule inverse Bremsstrahlung absorption coefficient is only valid for temperatures less than 4321.5 K. In addition, Mertogul's formula was derived for hydrogen plasma, a deviation from our interest in airbreathing laser propulsion. Nevertheless, Mertogul's formula is included in this study to compare the relative importance of these three types of inverse Bremsstrahlung absorption.

Results and Discussion

Thermodynamics for Multiply Ionized Air Plasma

Figure 2 shows the computed entropies and heat capacities for N, N^+, N^{+2}, N^{+3}, N^{+4}, N^{+5}, and N^{+6}, whereas Fig. 3 shows those for O, O^+, O^{+2}, O^{+3}, O^{+4}, O^{+5}, O^{+6}, and O^{+7} at 1 atm. The entropy curves are S shaped, whereas the heat capacity curves are bell shaped. The location of the action, that is, the value of the thermodynamic properties that change the most, is a function of the heat of formation. The peak value of the heat capacity increases with temperature as the number of stripped electrons increases. Note that the peak heat capacities are determined by the lowering of ionization potentials; a constant peak value near 85.45 is obtained for all of the multiply ionized atoms if the lowering of the ionization potential is set to zero.

Effect of Multiply Ionized Air Plasma Absorption of Laser Radiation at 1 Atmosphere

Thermodynamic functions generated from the properties shown in Figs. 2 and 3 are inputs to the general thermochemical system where equilibrium composition is computed to study the effect of multiply ionized air plasma absorption of laser radiation by use of a minimization of free energy procedure. Figure 4 shows the air plasma equilibrium composition at 1 atm, considering single ionization only. As temperature increases, the parent molecules (N_2 and O_2) disappear, and intermediate molecule (NO) and neutral atoms (N and O) emerge. Then they disappear, whereas electron e^- and ions N^+ and O^+ emerge; eventually, only the electron and ions are left in the system. The mole fractions of all three species level off at about 32,000 K. The final electron mole fraction of 0.5 is the result of single ionization. Note that the concentrations of NO^+, N_2^+, and O_2^+ are negligible.

Figure 5 shows a comparison of computed air absorption coefficients for CO_2 laser radiation using the information from Fig. 4. The computed absorption coefficients are extremely low at low temperatures and rise sharply with increasing temperature around 8000 K. Also plotted in Fig. 5 are points from Fig. 6.18 of Raizer and

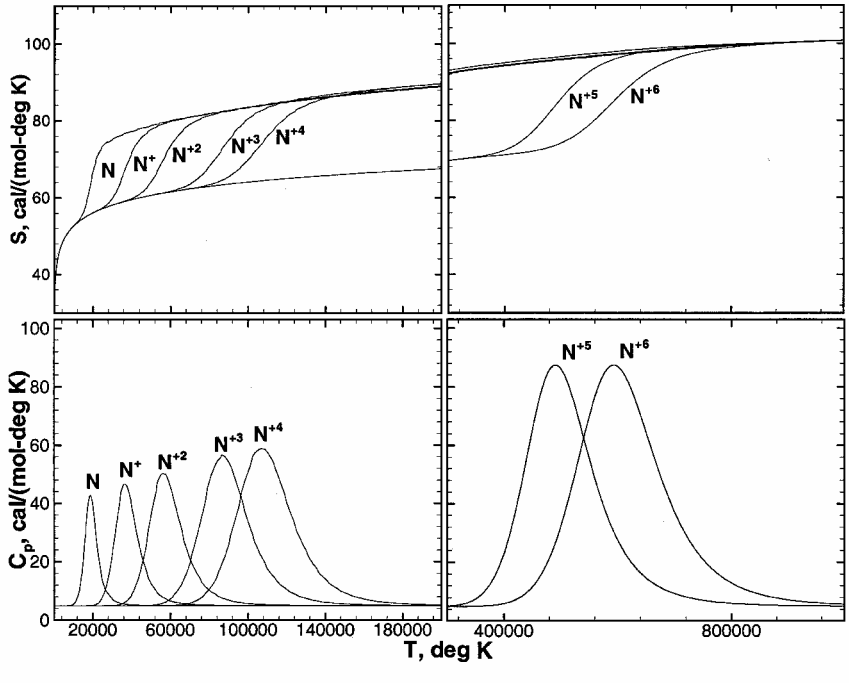

Fig. 2 Entropies and heat capacities for multiply ionized nitrogen atoms at 1 atm.

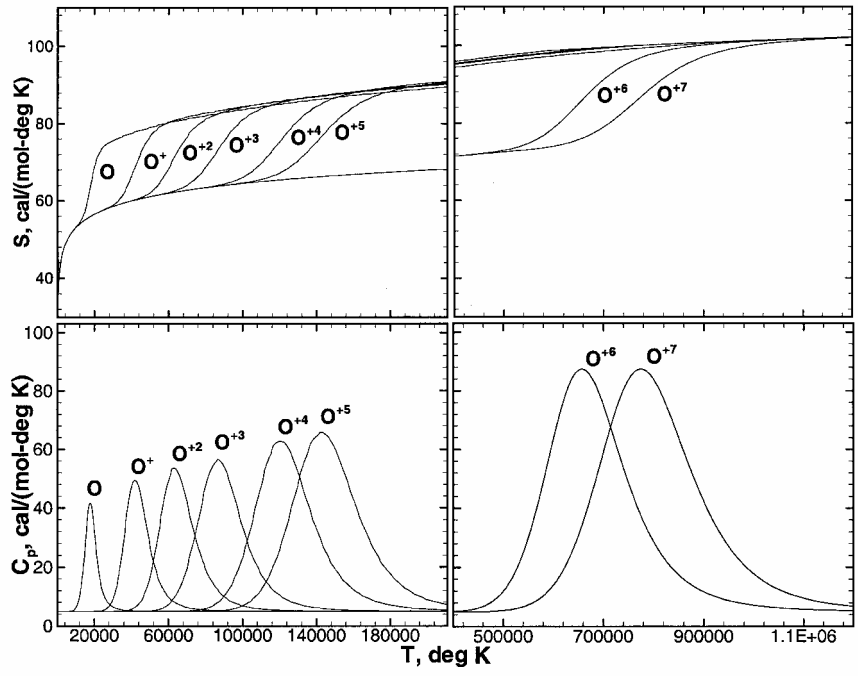

Fig. 3 Entropies and heat capacities for multiply ionized oxygen atoms at 1 atm.

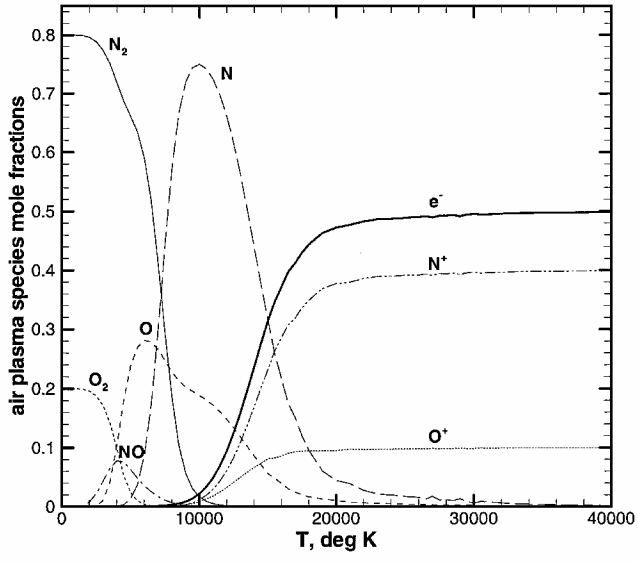

Fig. 4 Singly ionized air plasma equilibrium composition using minimization of free energy at 1 atm.

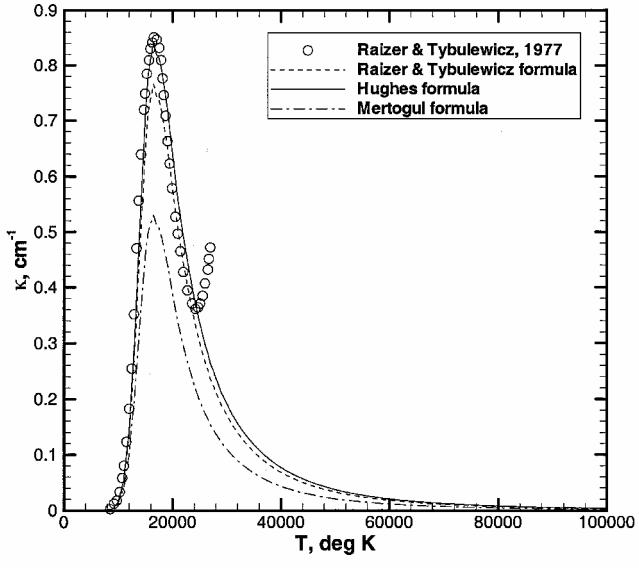

Fig. 5 Comparison of air absorption coefficients at 1 atm.

Tybulewicz[13] while allowing for (partial) double ionization. Precomputations have shown that the curves from all three formulas are very similar qualitatively. They peak at about the same temperature of 17,000 K, except the peak values are different because of the obvious difference in their basic formulations. Note that same Gaunt factor is used for both the Hughes[20] formula and the Raizer and Tybulewicz[13] formula. The peak value of the Hughes[20] formula is always the highest, followed by that of Raizer and Tybulewicz,[13] whereas that of Mertogul[21] is the lowest. The peak value is a direct result of single ionization, and it is a function of electron pressure (number density), which in turn is a function of the thermodynamics. For convenience, we have elected to modify the Gaunt factor such that the peak value of single ionization of the Hughes[20] formula matches that of the peak value of points read from Fig. 6.18 of Raizer and Tybulewicz.[13] The common characteristic of the three computed curves is that they drop monotonically from the maximum as the system completes the single ionization, eventually approaching zero beyond 100,000 K. None of them exhibits a rise at 25,000 K as indicated by the (partial) second ionization curve of Raizer and Tybulewicz,[13] which indicates an underestimation of the absorption (or energy conversion) with a single ionization system if the second rise due to double ionization can be reproduced.

Figure 6 shows a comparison of the electron–ion, electron–atom, and electron–molecule inverse Bremsstrahlung absorption coefficients using the Mertogul[21] formula. The electron–ion absorption is apparently the dominant mechanism, whereas both electron–atom and electron–molecule mechanisms appear negligible. Remember that (from Fig. 4) the molecules disappear around 10,000 K, whereas neutral atoms emerge around 2000 K and disappear around 30,000 K. Therefore, the free–free inverse Bremsstrahlung absorption is indeed the dominant absorption process among the three, as noted by Raizer and Tybulewicz.[13] Because of its flexibility, the electron–ion inverse Bremsstrahlung Hughes[20] formula is used exclusively for the following parametric studies and rewritten for multispecies, multiply ionization as

$$\kappa_\omega = \frac{n_e\left(\sum_i Z_i^2 n_i\right) q^6 g[1-\exp(-\hbar\omega/\kappa_B T)]}{\mu 6\varepsilon_0^3 c\hbar\omega^3 m_e^2}\left(\frac{m_e}{6\pi\kappa_B T}\right)^{\frac{1}{2}} \qquad (20)$$

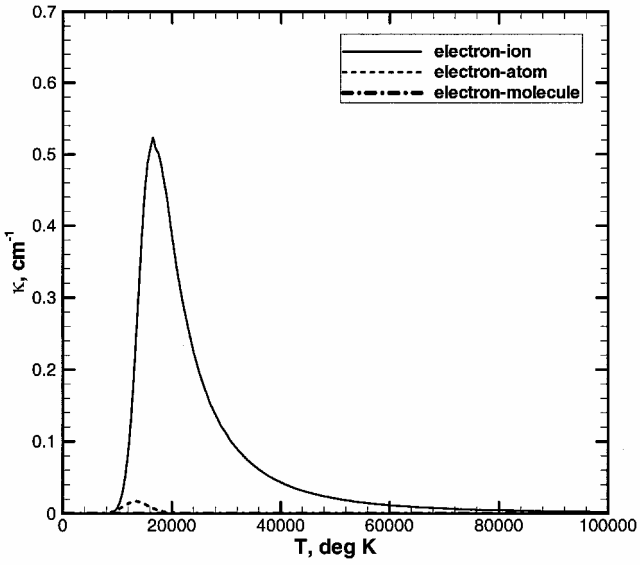

Fig. 6 Comparison of the electron–ion, electron–atom, and electron–molecule inverse Bremsstrahlung air absorption coefficients at 1 atm using Mertogul formula.[21]

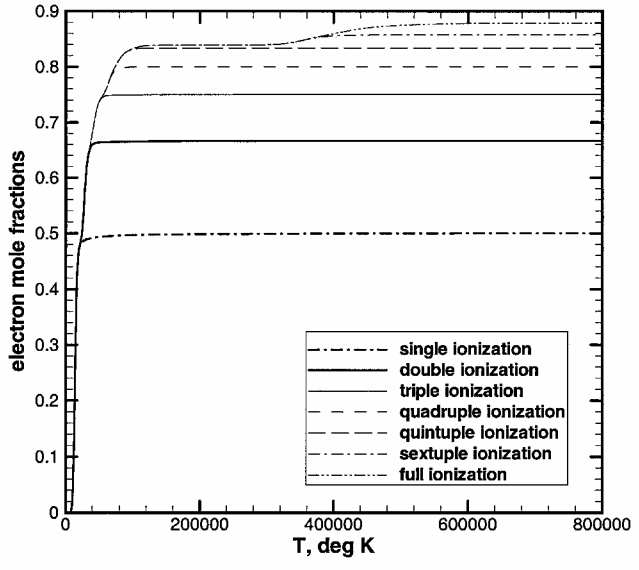

Fig. 7 Electron mole fractions using Saha equilibrium up to full ionization at 1 atm.

with a modified Gaunt factor

$$g = 0.63\ell_n\left[27(T/10^4)^{\frac{4}{3}}p_e^{-\frac{1}{3}}\right] \tag{21}$$

To provide the number densities of electron and multiply ionized atoms for the absorption computation, a series of equilibrium computations were performed up to full ionization. The simpler first thermochemical system containing only atoms and ions was chosen, and the equilibrium state was achieved by solving the Saha equations. Figure 7 shows the computed electron mole fractions. The electron mole fractions increase from 0.5 for single ionization to 0.67, 0.75, 0.8, 0.83, 0.86, and 0.88 for double, triple, quadruple, quintuple, sextuple, and full ionizations, respectively. The sextuple and full ionization are not invoked until about 400,000 K. Figure 8 shows the computed electron number densities. At high temperatures, the electron number densities increase as the degree of ionization increases, but the increase becomes marginal beyond quadruple ionization. Figure 9 shows the computed air absorption coefficient until full ionization. This time, there is an apparent second peak caused by the electrons produced with second ionization. The rise part of the second peak matches reasonably well with that of Raizer and Tybulewicz.[13] As the system completes the second ionization,

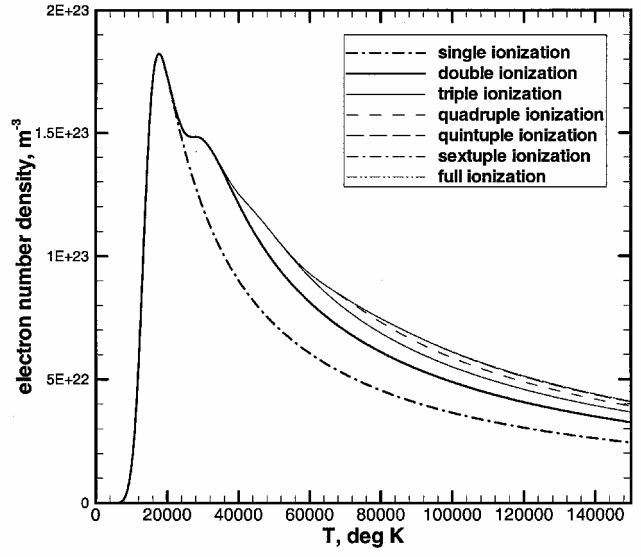

Fig. 8 Electron number densities using Saha equilibrium up to full ionization at 1 atm.

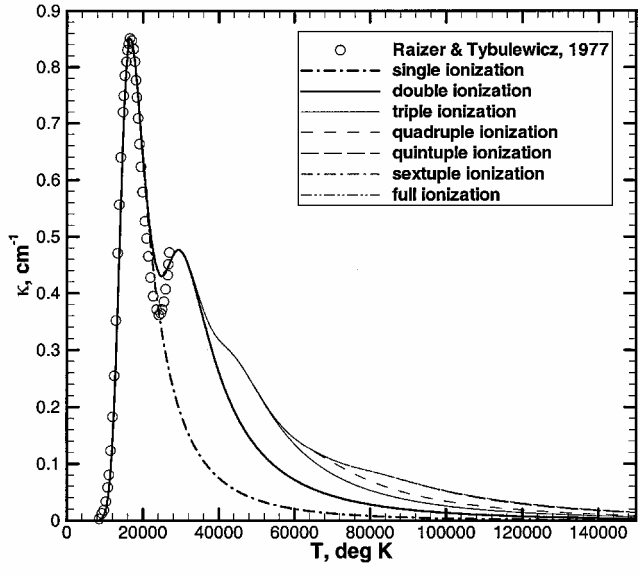

Fig. 9 Air absorption coefficients using Saha equilibrium up to full ionization at 1 atm.

the absorption curve again rises due to the electrons produced by the triple ionization, although there is no apparent third peak, and so on. Again, the amount of increase decreases with the increased degree of ionization. Again it is estimated that the increase of absorption coefficient becomes marginal beyond quadruple ionization. Note that the area under the quadruple (or full) ionization curve is about twice that of the single ionization. Figure 10 shows the computed equilibrium air plasma species composition during full ionization. Multiple peaks of multiply ionized N and O atoms appear as temperature increases, whereas the electron mole fraction appears to level off beyond quadruple ionization and does not rise again until sextuple ionization (or 300,000 K).

As discussed earlier, the improvement in the computed air plasma absorption coefficient becomes marginal beyond quadruple ionization. This is important for computational plasma aerodynamics analysis because the computational cost is approximately proportional to the square of the number of species considered. Figure 11 shows the quadruply ionized air plasma equilibrium composition, using the second thermochemical system and minimization of free energy for achieving the equilibrium state. The multiple peaks of species N^+, N^{+2}, N^{+3}, O^+, O^{+2}, and O^{+3} caused by single, double, and triple ionizations are very similar to those of Fig. 10. The plateau value of the electron mole fraction also approximates that of Fig. 10

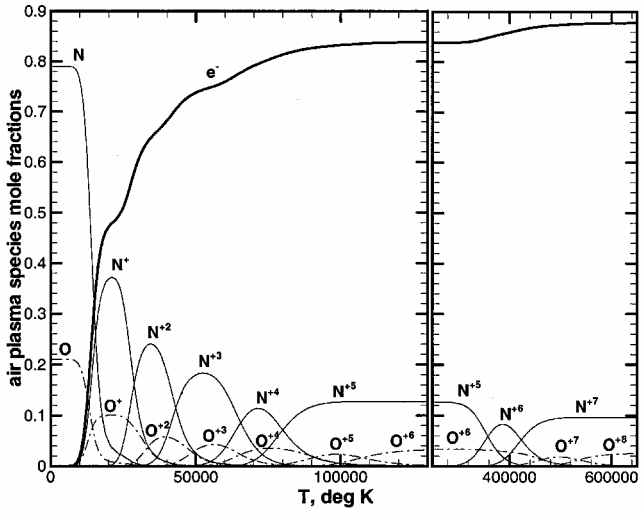

Fig. 10 Fully ionized air plasma composition using Saha equilibrium at 1 atm.

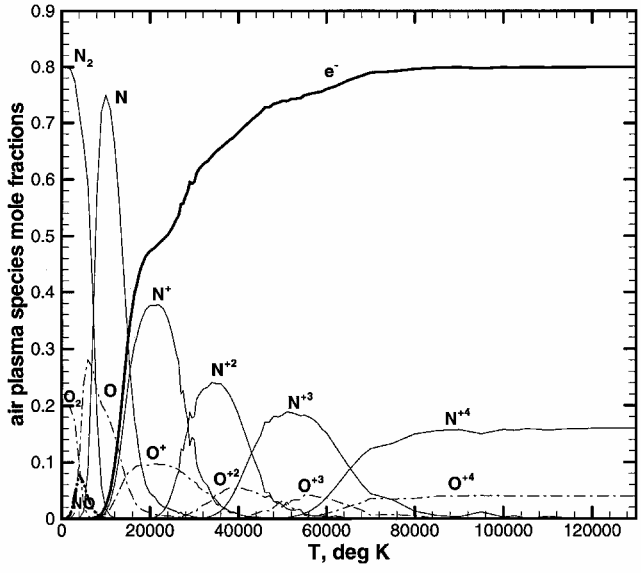

Fig. 11 Quadruply ionized air plasma equilibrium composition using minimization of free energy at 1 atm.

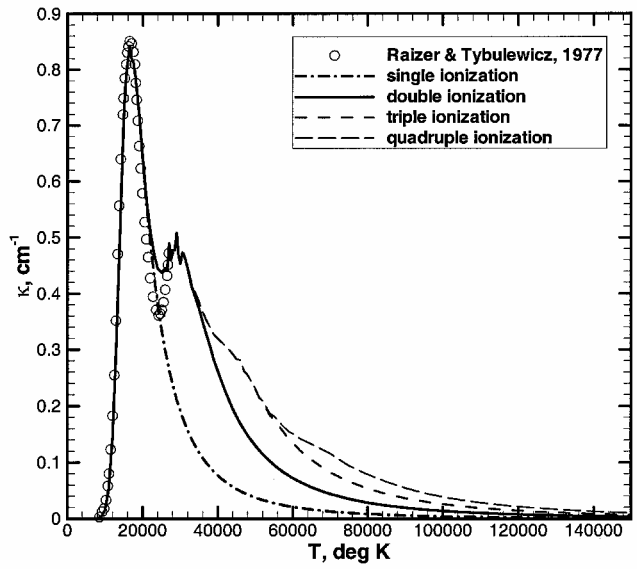

Fig. 12 Air absorption coefficients using minimization of free energy equilibrium up to quadruple ionization at 1 atm.

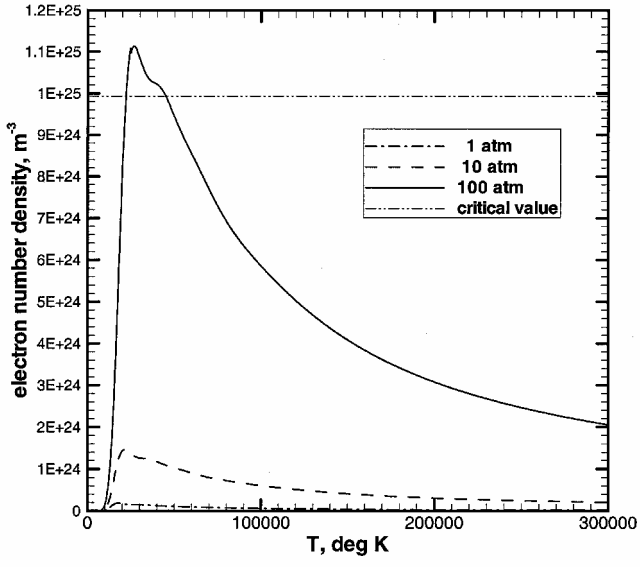

Fig. 13 Comparison of electron number densities using Saha equilibrium and full ionization.

for quadruple ionization. The information from Fig. 11 is then used to compute the absorption coefficient as shown in Fig. 12. The curves of single, double, triple, and quadruple ionizations match very well with those shown in Fig. 9, which demonstrates that the quadruple ionization effect can be reproduced in computational plasma dynamics analysis using curve-fitted thermodynamic functions.

Effect of Pressure on Multiply Ionized Air Plasma Absorption of Laser Radiation

During optical breakdown of air at sea level, the pressure rises, as indicated in Ref. 11. This pressure rise increases the absorption coefficient. On the other hand, the ambient pressure decreases as altitude increases. That pressure attenuation decreases the absorption coefficient. Therefore, the effect of pressure needs to be addressed. This is accomplished by performing a series of assigned temperature and pressure computations, by the use of the Saha equation for achieving the equilibrium state with the first thermochemical system, assuming full ionization. Figure 13 shows the computed electron number densities at these three pressures. The peak electron number density at 100 atm is about an order of magnitude higher than that of the 10 atm. In turn, the peak electron number density at 10 atm is about an order of magnitude higher than that at 1 atm. The computed electron number density exceeds the critical value at 100 atm for temperatures ranging from 20,000 to 45,000 K. Plasma resonance occurs when the critical electron number density is reached. A critical electron density above which the laser beam is totally reflected can be obtained by equating the angular frequency of the incident laser with that of the plasma.[11]

Figure 14 shows the computed air absorption coefficients at 1, 10, and 100 atm. Note that the absorption coefficient is divided by the square of pressure. The computed curves agree reasonably well with those of Raizer and Tybulewicz[13] and essentially expand their partial double ionization curve to full ionization. The computed double ionization peak occurs at about 30,000, 35,000, and 40,000 K for 1, 10, and 100 atm, respectively. The curves flatten out as the pressure increases. Figure 15 shows the computed full ionization air absorption coefficients at 0.01, 0.1, 1, 10, and 100 atm. The second peak due to double ionization occurs at around 23,000 and 27,000 K, for pressures of 0.01 and 0.1 atm, respectively. The absorption coefficient increases about two orders of magnitude each time as it goes from 1 to 10 atm and from 10 to 100 atm, respectively. It reduces about two orders of magnitude each time as it drops from 1 to 0.1 atm and from 0.1 to 0.01 atm, respectively.

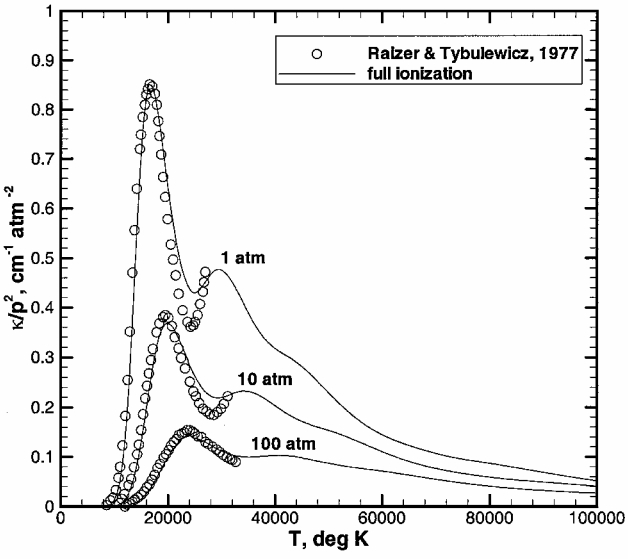

Fig. 14 Comparison of air absorption coefficients at 1, 10, and 100 atm.

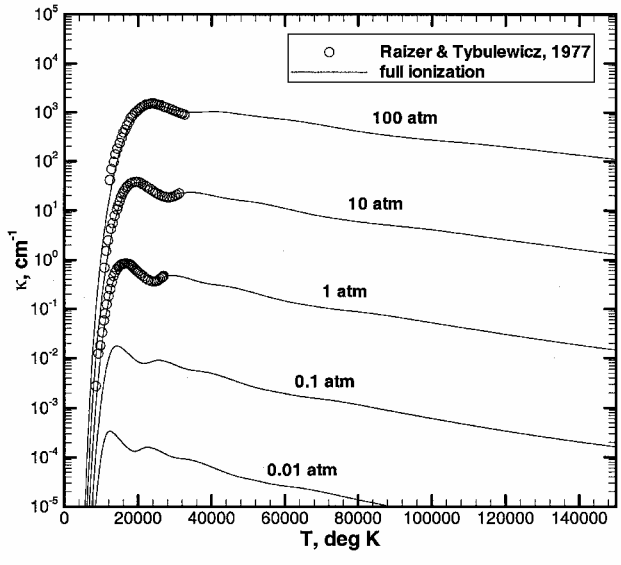

Fig. 15 Comparison of air absorption coefficients at 0.01, 0.1, 1, 10, and 100 atm.

Conclusions

A thermophysics characterization of inverse Bremsstrahlung absorption of laser radiation is performed. High-temperature thermochemical properties of multiple ionized air plasma species are generated using hydrogenic approximation of the electronic partition function. Three formulas for absorption are studied, and a general formula is derived for multispecies, multiple ionization absorption computation. A series of thermal equilibrium computations are performed to show the effect of multiple ionization on the free electron concentration and on the inverse Bremsstrahlung absorption coefficient. The computed second ionization absorption coefficient agrees reasonably well with that of literature. The area under the quadruple (or full) ionization curve of absorption is about twice that of the single ionization, which demonstrates the importance of multiple ionization on the modeling of energy conversion processes. The effect of pressure on the air plasma absorption coefficient is presented. The result of this study can be applied directly to the computational plasma aerodynamics modeling of laser propulsion physics.

Acknowledgments

The first author extends thanks to John Cole of Revolutionary Propulsion Research for supporting this study. He also thanks Yen-Sen Chen and Jiwen Liu of Engineering Science, Inc., for discussions on the laser absorption coefficients. The computational procedure for solving the hydrogenic approximation of the partition function and the Saha equations was originally developed by Dennis Keefer's research group at the University of Tennessee Space Institute. The first author also wishes to thank Jelai Wang for reading the manuscript.

References

[1]Kantrowitz, A., "Propulsion to Orbit by Ground-Based Lasers," *Astronautics and Aeronautics*, Vol. 10, No. 5, 1972, pp. 74–76.

[2]Pirri, A. N., Monsler, M. J., and Nebolsine, P. E., "Propulsion by Absorption of Laser Radiation," *AIAA Journal*, Vol. 12, No. 9, 1974, pp. 1254–1261.

[3]Glumb, R. J., and Krier, H., "Concepts and Status of Laser-Supported Rocket Propulsion," *Journal of Spacecraft and Rockets*, Vol. 21, No. 1, 1984, pp. 70–79.

[4]Brandstein, A., and Levy, Y., "Laser Propulsion System for Space Vehicles," *Journal of Propulsion and Power*, Vol. 14, No. 2, 1998, pp. 261–269.

[5]Phipps, C. R., Reilly, J. P., and Campbell, J. W., "Optimum Parameters for Laser Launching Objects into Low Earth Orbit," *Laser and Particle Beams*, Vol. 18, No. 4, 2000, pp. 661–695.

[6]Myrabo, L. N., "World Record Flights of Beam Riding Rocket Lightcraft: Demonstration of 'Disruptive' Propulsion Technology," AIAA Paper 2001-3798, July 2001.

[7]Bohn, W. L., "Laser Lightcraft Performance," *High Power Laser Ablation II*, edited by C. R. Phipps and M. Niino, Vol. 3885, Society of Photo-Optical Instrumentation Engineers, Bellingham, WA, 2000, pp. 48–53.

[8]Molvik, G. A., Choi, D., and Merkle, C. L., "A Two-Dimensional Analysis of Laser Heat Addition in a Constant Absorptivity Gas," *AIAA Journal*, Vol. 23, No. 7, 1985, pp. 1053–1060.

[9]Jeng, S.-M., and Keefer, D., "Theoretical Evaluation of Laser-Sustained Plasma Thruster Performance," *Journal of Propulsion*, Vol. 5, No. 5, 1989, pp. 577–581.

[10]Conrad, R., Raizer, Y. P., and Surzhikov, S. T., "Continuous Optical Discharges Stabilized by Gas Flow in Weakly Focused Laser Beam," *AIAA Journal*, Vol. 34, No. 8, 1996, pp. 1584–1588.

[11]Wang, T.-S., Chen, Y.-S., Liu, J., Myrabo, L. N., and Mead, F. B., Jr., "Advanced Performance Modeling of Experimental Laser Lightcraft," *Journal of Propulsion and Power*, Vol. 18, No. 6, 2002, pp. 1129–1138.

[12]Zel'dovich, Y. B., and Raizer, Y. P., *Physics of Shock Waves and High Temperature Hydrodynamic Phenomena*, edited by W. D. Hayes and R. F. Probstein, Vol. 1, Academic Press, New York, 1966, pp. 201–207.

[13]Raizer, Y. P., and Tybulewicz, A., "Laser-Induced Discharge Phenomena," *Studies in Soviet Science*, edited by G. C. Vlases and Z. A. Pietrzyk, Consultants Bureau, New York, 1977, pp. 241–243.

[14]Gordon, S., and McBride, B. J., "Thermodynamic Data to 20,000 K for Monatomic Gases," NASA TP 1999-208523, June 1999.

[15]Richter, J., "Radiation of Hot Gases," *Plasma Diagnostics*, edited by W. Lochte-Holtgreven, Wiley, New York, 1968, pp. 1–32.

[16]Gordon, S., and McBride, B. J., "Computer Program for Calculation of Complex Chemical Equilibrium Compositions and Applications," NASA RP 1311, 1996.

[17]Park, C., "Review of Chemical–Kinetic Problems of Future NASA Missions, Part 1: Earth Entries," *Journal of Thermophysics and Heat Transfer*, Vol. 7, No. 3, 1993, pp. 385–398.

[18]Gurvich, L. V., Veyts, I. V., and Alcock, C. B., *Thermodynamic Properties of Individual Substances*, 4th ed., Pt. 2, Hemisphere, New York, 1989, pp. 3–6, 194–197.

[19]Jaffe, R., "The Calculation of High-Temperature Equilibrium and Nonequilibrium Specific Heat Data for N_2, O_2, and NO," AIAA Paper 87-1633, June 1987.

[20]Hughes, T. P., *Plasma and Laser Light*, Wiley, New York, 1975, pp. 44, 45.

[21]Mertogul, A. E., "Modeling and Experimental Measurements of Laser Sustained Hydrogen Plasmas," Ph.D. Dissertation, Mechanical Engineering Dept., Univ. of Illinois, Urbana–Champaign, IL, Feb. 1993.

[22]Stallcop, J. R., "Absorption of Laser Radiation in a H–He Plasma. I. Theoretical Calculation of the Absorption Coefficient," *Physics of Fluids*, Vol. 17, No. 4, 1974, pp. 751–758.

[23]Karzas, W. J., and Latter, R., "Electron Radiative Transitions in a Coulomb Field," *Astrophysical Journal, Supplement Series*, Vol. 6, Supplement No. 55, 1961, pp. 167–211.

[24]Stallcop, J. R., "Absorption of Infrared Radiation by Electrons in the Field of a Neutral Hydrogen Atom," *Astrophysical Journal*, Vol. 187, No. 1, 1974, pp. 178–183.

[25]Caledonia, G. E., Wu, P. K. S., and Pirri, A. N., "Radiation Energy Absorption Studies for Laser Propulsion," NASA CR-134809, March 1975.

[26]Dalgarno, A., and Lane, N. F., "Free-Free Transitions of Electrons in Gases," *Astrophysical Journal*, Vol. 145, No. 2, 1966, pp. 623–633.